## Photovoltaic properties of Bi$_2$FeCrO$_6$ films epitaxially grown on (100)-oriented silicon substrates†

R. Nechache,*[a,b] W. Huang,[a] S. Li[a] and F. Rosei*[a,c,d]

We demonstrate the promising potential of using perovskite Bi$_2$FeCrO$_6$ (BFCO) for niche applications in photovoltaics (PV) (*e.g.* self-powered sensors that simultaneously exploit PV conversion and multiferroic properties) or as a complement to mature PV technologies like silicon. BFCO thin films were epitaxially grown on silicon substrates using an MgO buffer layer. Piezoresponse force microscopy measurements revealed that the tensile strained BFCO phase exhibits a polarization predominantly oriented through the in-plane direction. The semiconducting bandgap of the ordered BFCO phase combined with ferroelectric properties, opens the possibility of a ferroelectric PV efficiency above 2% in a thin film device and the use of ferroelectric materials simultaneously as solar absorber layers and carrier separators in PV devices. A large short circuit photocurrent density of 13.8 mA cm$^{-2}$ and a photovoltage output of 0.5 V are typically obtained at FF of 38% for BFCO devices fabricated on silicon. We believe that the reduced photovoltage is due to the low diffusion length of photogenerated charge carriers in the BFCO material where the ferroelectric domains are predominately oriented in-plane and thus do not contribute efficiently to the photocharge separation process.

Bismuth-based inorganic double perovskites, such as BiFeO$_3$ (BFO) and Bi$_2$FeCrO$_6$ (BFCO) have been recently widely studied because of their multiferroic behavior as well as promising photovoltaic (PV) properties.[1–5] These materials exhibit a non-centrosymmetric crystal structure with strong inversion symmetry breaking that yields a spontaneous electric polarization.

[a]*INRS – Centre Énergie, Matériaux et Télécommunications, Boulevard Lionel-Boulet, Varennes, Québec J3X 1S2, Canada. E-mail: nechache@emt.inrs.ca, rosei@emt.inrs.ca*

[b]*Département de Génie Electrique, Ecole de technologie supérieure, 1100 rue Notre-Dame Ouest, H3C 1K3 Montréal, QC, Canada*

[c]*Institute for Fundamental and Frontier Science University of Electronic Science and Technology of China, Chengdu 610054, P. R. China*

[d]*Center for Self-Assembled Chemical Structures, McGill University, H3A 2K6 Montreal, Quebec, Canada*

†Electronic supplementary information (ESI) available. See DOI: 10.1039/c5nr08819d

The latter promotes the required separation of photo-excited carriers and permits photovoltage values that can exceed (up to a factor of 5) the bandgap of the materials.[1,6] In principle, the use of this material as an active layer in PV devices may allow us to achieve conversion efficiencies beyond the maximum values predicted in a conventional semiconductor p–n junction solar cell.[7] Very high PV efficiencies (up to 70%) were theoretically predicted in devices based on such materials.[7] Among these systems, BFCO is highly promising because it has been shown to exhibit a conversion efficiency of up to a breakthrough value of 8.1% under 1 Sun illumination in thin film form.[8] Detailed investigations also highlighted the strong dependence of the sign and magnitude of the generated photocurrent on the direction of the ferroelectric (FE) polarization.[8] A unidirectional ferroelectric polarization maximizes the driving force of the photogenerated charges, resulting in a more efficient charge separation process. In addition, the optical properties of BFCO thin films can be modulated and optimized to complement those of crystalline silicon and other thin films used in devices such as n-CdS/p-CuInSe$_2$ (CIS), n-CdS/p-CuIn$_{1-x}$Ga$_x$Se$_2$ (CIGS), and Cu$_2$ZnSnSe$_4$ (CZTSe), when used as a top cell in a tandem junction[9,10] of the tandem architecture which was predicted to potentially lead to efficiencies beyond the Shockley–Queisser limit estimated in a single junction device.[11] Due to Auger recombination, which mainly limits the photocharge carrier lifetime,[12] a significant increase in efficiency for crystalline silicon cells is unlikely. In addition, the development of wide-bandgap top cells for tandem junctions based on silicon and thin film PV cells still remains a challenge for future generation PV devices.[9,13] In fact, this device architecture requires careful management of the absorbed radiation, where short-wavelength light should be preferentially absorbed in the top cell and long-wavelength light is to be transmitted unrestricted to the bottom cell. Thanks to the tunable optical properties and electrical conductivity of perovskite oxides, placing such a material on top of a silicon cell is expected to enhance the power conversion efficiency (PCE) of existing PV technologies with simultaneous cost effectiveness.[10]

As previously shown, Fe/Cr cationic ordering plays an important role in the PV effect in BFCO films, as it allows us to tune the bandgap, thereby growing thin films that collect photons from different portions of the solar spectrum.[4,8] High short-circuit photocurrent densities (1–23 mA cm$^{-2}$) are observed when the films exhibit high cationic ordering. Since this ordering is possible only in epitaxial films, the epitaxial growth of highly ordered BFCO on Si or CIS is a critical challenge to achieve high efficiency tandem junction device configurations.

Due to the various factors that hinder epitaxial growth, such as lattice mismatch, chemical reactions taking place between overlayer constituents and the substrate and interdiffusion, several oxides cannot be grown directly on silicon substrates with the desired crystalline phase. To achieve ordered growth, a buffer layer is usually required between the oxide and the Si substrate. Several oxide films, including MgO,[14] SrTiO$_3$,[15] SrO[16] and yttria-stabilized zirconia[17] have been used as buffer layers. MgO has been used to grow buffer layers on Si(001) because it exhibits several interesting properties, including the ability to function as a diffusion barrier, high thermal stability and good electrical insulation.[14] Various methods have been used to deposit epitaxial MgO(001) films on Si(001) substrates, including pulsed laser deposition (PLD)[14] and magnetron sputtering.[18]

Here we report the epitaxial growth of BFCO films on SrRuO$_3$ (SRO)/SrTiO$_3$:Nb (NSTO) thin film electrodes using an MgO buffer layer on (100)-oriented crystalline Si, using PLD. X-ray diffraction (XRD) shows that the BFCO films crystallize in a highly c-oriented single phase. Piezoresponse force microscopy (PFM) reveals that the films exhibit ferroelectric properties with domains mainly oriented in-plane. We measured power conversion efficiencies up to 2.65% in these films under 1 Sun illumination. A large short circuit photo-current density of 13.8 mA cm$^{-2}$ and a photovoltage output of 0.5 V are typically obtained for such devices at FF of 38%. While these values are not sufficiently high for a stand-alone PV technology, our work demonstrates the promising potential of using multiferroic oxide materials for niche applications in PV (e.g. self-powered sensors that simultaneously exploit PV conversion and multiferroic properties) or as a complement to mature technologies like silicon PV.

The films used in this study were deposited by PLD using a multi-target carousel. This system was constructed on the basis of the parameters required to obtain high quality single- or multi-layer films. The system was built with four 1 inch diameter target holders leading to the consecutive deposition of up to four materials without breaking the vacuum, which results in layer interfaces with limited defect densities and contaminations (e.g. carbon) which might dramatically affect device performances. The target–substrate distance and background vacuum were 6 cm and 10$^{-7}$ mTorr, respectively. An Excimer KrF laser with a wavelength of 248 nm and 15 ns pulse duration was employed. The used energy density was in the range of 1–2 J cm$^{-2}$, resulting in a growth rate of 0.1–0.2 Å per pulse. Prior to deposition, the silicon substrates were consecutively cleaned using oxygen plasma and buffered HF treatments to eliminate any organic contamination and the native Si oxide, respectively.

200 nm thick BFCO thin films were grown by PLD on 45 nm thick MgO buffered Si(001) substrates. Intermediate buffer layers are needed to promote the epitaxial growth of perovskite oxide thin films on silicon and accommodate the large lattice mismatch, of about 6.5% between the perovskite material and silicon. To compensate for the differences in bonding, chemistry, and coordination between silicon and the oxide layer, we grew epitaxially a 45 nm thick MgO buffer layer onto a Si(100) substrate. A detailed investigation of the thickness dependence of MgO film properties reveals that the MgO layer with this thickness exhibits good crystal quality with the smoothest surface. MgO films with increasing thickness (above 45 nm) result in a textured crystalline phase, as inferred from the presence of (111) and (220) reflections in the XRD patterns. To ensure heteroepitaxial growth and maintain the interfacial strain, a thin perovskite multilayer of 15 nm SRO/ 35 nm NSTO was used as the bottom electrode. The strain stabilizes the cationic ordering in BFCO films, which is a key parameter for its absorption and PV properties.[4,19] Details of deposition parameters are listed in Table SI.† Since NSTO films are optically transparent with lower conductivity (cf. Fig. S1†), we integrated the SRO layer to improve the conductivity of the bottom electrode to serve as a back rear reflective layer for BFCO-based PV devices and demonstrating thus the maximum power conversion energy of BFCO that can be obtained in this device architecture. The integration of BFCO in a tandem cell with Si for example, will not need the SRO and the transmitted light will therefore be absorbed by a Si based bottom cell.

X-ray θ–2θ spectra only display (0 0 l) peaks, confirming the c-axis orientation of the oxide stack, yielding a BFCO c-axis lattice parameter of 0.391 nm (Fig. 1a). Rocking curve measurements reveal the high crystalline quality of the BFCO layer with a full width half maximum (FWHM) of 0.3° around the BFCO (001) peak and FWHM of 0.05° for Si(004). The FWHM measured for films on Si(001) substrates is closer to that for BFCO films grown on (001) NSTO (001) substrates,[4] suggesting that the crystalline quality of BFCO films on Si(001) (using a suitable buffer) is as good as for those grown on NSTO (001) substrates. Detailed diffraction pattern analyses (φ-scans, Fig. 1b) confirm the fourfold symmetry of the epitaxial relationship between the oxide layers and the substrate: BFCO [001]//SRO [001]//NSTO [001]//Si [001] and [100]//SRO[100]/ NSTO[100]/Si[100].

The Fe/Cr cationic ordering in BFCO films can be characterized by performing asymmetrical θ–2θ scans around (111) STO reflections (Fig. 1c).[19] In addition to the main single perovskite (111) reflection (around 39.8°), periodic peaks at 2θ = 19.4 and 60.9° are observed indicating the doubling of the BFCO unit cell along this crystal direction as predicted by theoretical calculations.[20] No similar peaks are found along other directions, such as e.g. (101).
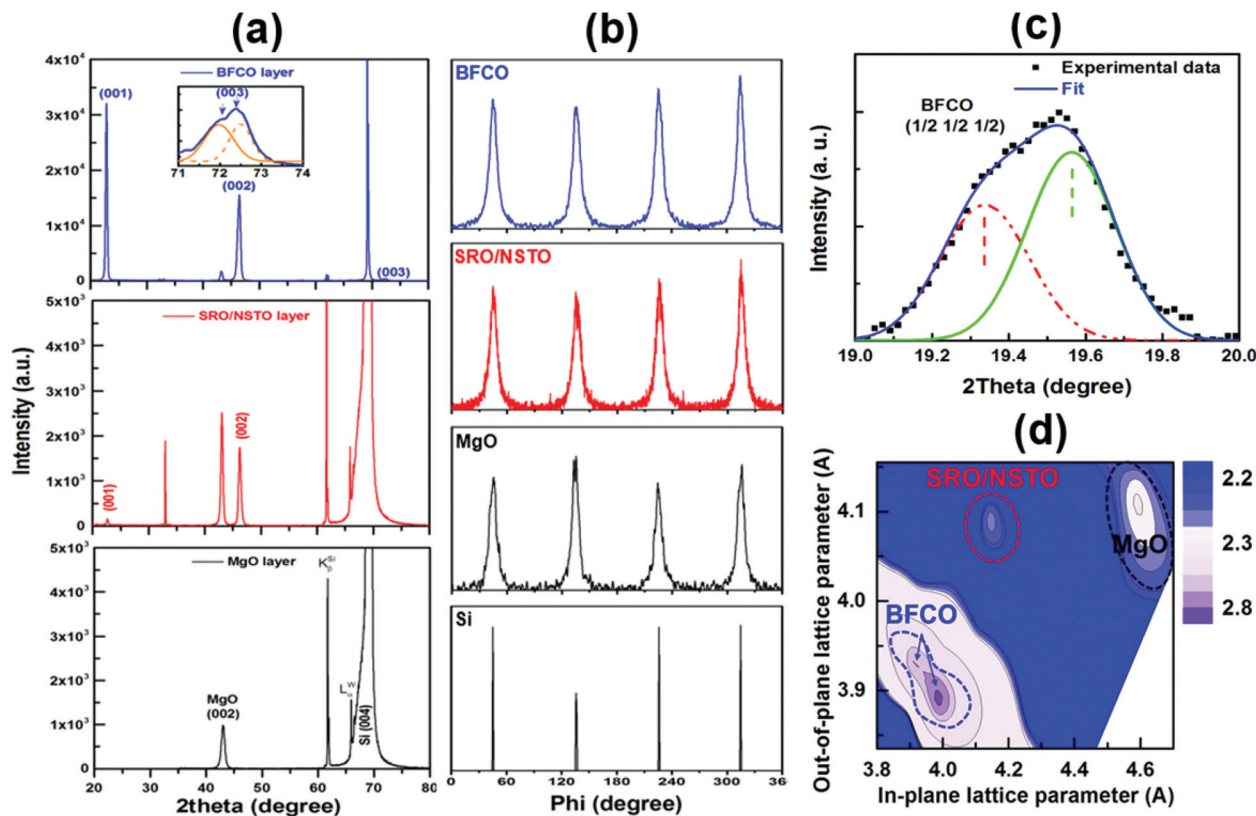
**Fig. 1** (a) XRD $\theta$–$2\theta$ scans of a BFCO (200 nm)/SRO (15 nm)/NSTO (35 nm) heterostructure (top) and of the MgO buffer layer on silicon (001) (bottom). (b) Corresponding $\varphi$-scan measurements around the (202) reflection of each layer involved in the oxide heterostructure. (c) The BFCO (1/2 1/2 1/2) reflection demonstrating Fe/Cr cationic ordering in the films. (d) RSM measurement around the (203) reflection of MgO.

To determine the in plane lattice parameters of each layer of the heterostructure, we performed reciprocal space mapping (RSM) around the (203) cubic reflection (*cf.* Fig. 1d). The obtained lattice parameters are summarized in Table SI.† MgO layers crystallize in the cubic structure with a lattice parameter around 0.42 nm, similar to the bulk value. The unit cell dimensions of 200 nm thick BFCO films grown on Si (100) are determined to be $a = b = 0.398$ nm and $c = 0.389$ nm. The lattice parameters were estimated within an experimental error of 2%. This indicates that the BFCO films are under tensile strain, promoted by the positive large lattice parameter mismatch of 6.5% with the Si unit cell. However, once we expect that 200 nm thick films will be fully relaxed the possible presence of multi-state valences for Fe and Cr in particular 2+ and 4+ states in the films might allow us to relieve the strain by the Jahn–Teller distortion of the oxygen octahedra surrounding these atoms. The reflection corresponding to the SRO phase was not visible in the RSM which might be overlapped by the other layer reflections.

A film roughness (r.m.s.) of about 2.35 nm was estimated from atomic force microscopy (AFM) topography images (Fig. 2a). This roughness value is close to those obtained for each layer involved in the heterostructure (images not shown here) suggesting the formation of smooth interfaces with a low

intermixing rate. The ferroelectric properties of BFCO films were locally investigated by PFM.[21,22] PFM measurements were performed using a Veeco Enviroscope AFM equipped with Pt/Ir coated ANSCM-PA probes from App Nano. We applied an AC voltage of 0.5 V at 26 kHz between the conductive tip and the SRO/NSTO bilayer of the sample located beneath BFCO and we detected the BFCO film surface induced piezoelectric vibrations using a lock-in amplifier from Signal Recovery (model 7265). In-plane (IP) and out-of-plane (OP) PFM images show inhomogeneous contrasts in the as deposited BFCO films (Fig. 2b and c). Grains with high (OP) and low (IP) PFM responses are visible. Hysteresis loops (Fig. 2d and e) were also recorded in both IP and OP directions by positioning the conductive AFM tip on different areas of the sample. The grains with high PFM response (HRG) exhibit hysteresis loops in both the IP and OP directions whereas only the IP loop is observed in the grains with low response (LRG). In addition, the IP-PFM signal of LRG is clearly higher than that observed for HRG. This indicates that the ferroelectric polarization of these grains is mainly oriented parallel to the film's surface. This is attributed to the tensile strain which extends the BFCO unit cell along the IP cubic crystal directions. For the HRG, the partial relaxation of the tensile-strain in the BFCO films results in the rotation of the ferroelectric polarization through the OP
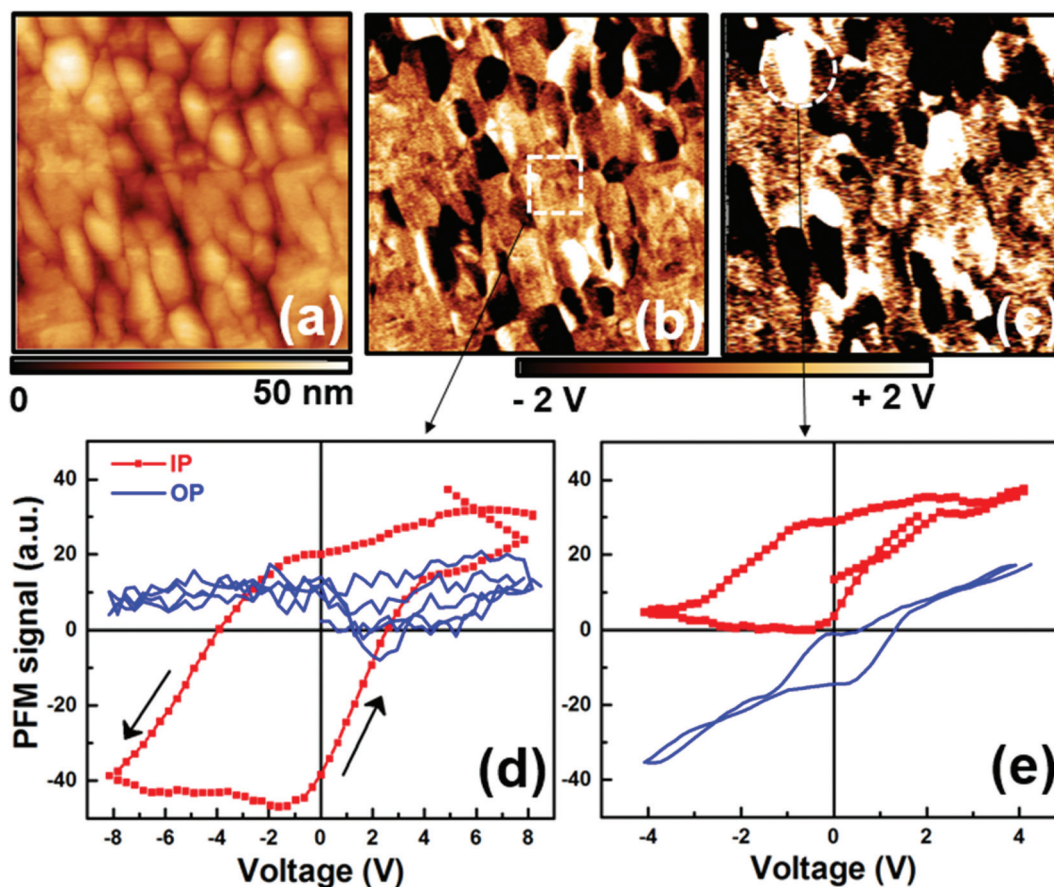
**Fig. 2** (a) 5 × 5 μm² AFM topography and the IP (b) and OP (c) PFM (amplitude cos phase) images of the heterostructure. (d) and (e) typical IP and OP-PFM signals recorded at different places on the sample, respectively.

plane direction thereby approaching that of bulk BFCO (*i.e.* 111). The difference of the strain state observed in BFCO films is evidenced by the $\theta$–$2\theta$ scan around the (003) reflection (inset of Fig. 1a), where two peaks at 71.9° and 72. 45° are visible. OP lattice parameters of 3.94 Å and 3.91 Å are estimated, which correspond to partially and highly strained BFCO phases (BFCO$_r$ and BFCO$_s$), respectively.

The optical absorption properties of BFCO films were characterized by spectroscopic ellipsometry performed at an incidence angle of 60° using a VASE ellipsometer (J.A. Woollam Company). A multilayer model consisting of air, single BFCO films, a SRO/NSTO bottom electrode and a (MgO/Si) substrate was used to describe the optical response (including the extinction coefficient $k$) of the heterostructure. The absorption coefficient $\alpha$ of the films was obtained from $k$ by using the following formula: $\alpha = 4\pi k/\lambda$, where $\lambda$ is the wavelength of the incident light. The bandgap $E_g$ of the films was calculated according to Tauc's relation using the following equation: $\alpha E = A(E - E_g)^n$, where $E$ is the photon energy, $A$ is a constant, and $n$ is equal to 1/2 or 2 for direct or indirect gap materials, respectively.[23] The data were compared with those obtained for the parent BFO and BiCrO₃ (BCO) films (BFCO could be obtained by co-deposition of BFO and BCO materials)

grown under the same conditions (*i.e.* substrate temperature and oxygen partial pressure).

Three absorption peaks at 385, 473 and 675 nm are visible for BFCO films. The optical band gap $E_g$ can be estimated from the absorption coefficient $\alpha$ (Fig. 3a). In our data, the lack of the characteristic shape of the $(\alpha E)^{1/2}$ *versus* the $E$ plot[24] and the presence of clear linear slopes in $(\alpha E)^2$ *versus* $E$ curves indicate that the bandgap of the films is direct (*cf.* Fig. 3b). Three linear slopes are visible in the $(\alpha E)^2$ curve and their linear extrapolation to zero allows us to determine the band gap values: 2.94, 2.41 and 1.55 eV respectively, within an experimental error of 2%. Following electronic structure calculations and the experimental absorption spectrum of similar materials with Fe/Cr in B-sites,[25,26] we assign the peaks ~1.55 eV (800 nm) and 2.14 eV (515 nm) to charge transfer excitations between Cr and/or O to Fe mixed d orbital Hubbard transitions that occur in locally ordered regions of the sample. Given a common coordination in the octahedral crystal field, the same mechanism is likely responsible for the observed red-shift in the BFCO film. The absorption around 2.92 eV is attributed to the contribution from Fe–O, Cr–O bonds either in BFCO disordered or ordered regions which can coexist in the films. This absorption is close to that of BFO[27]
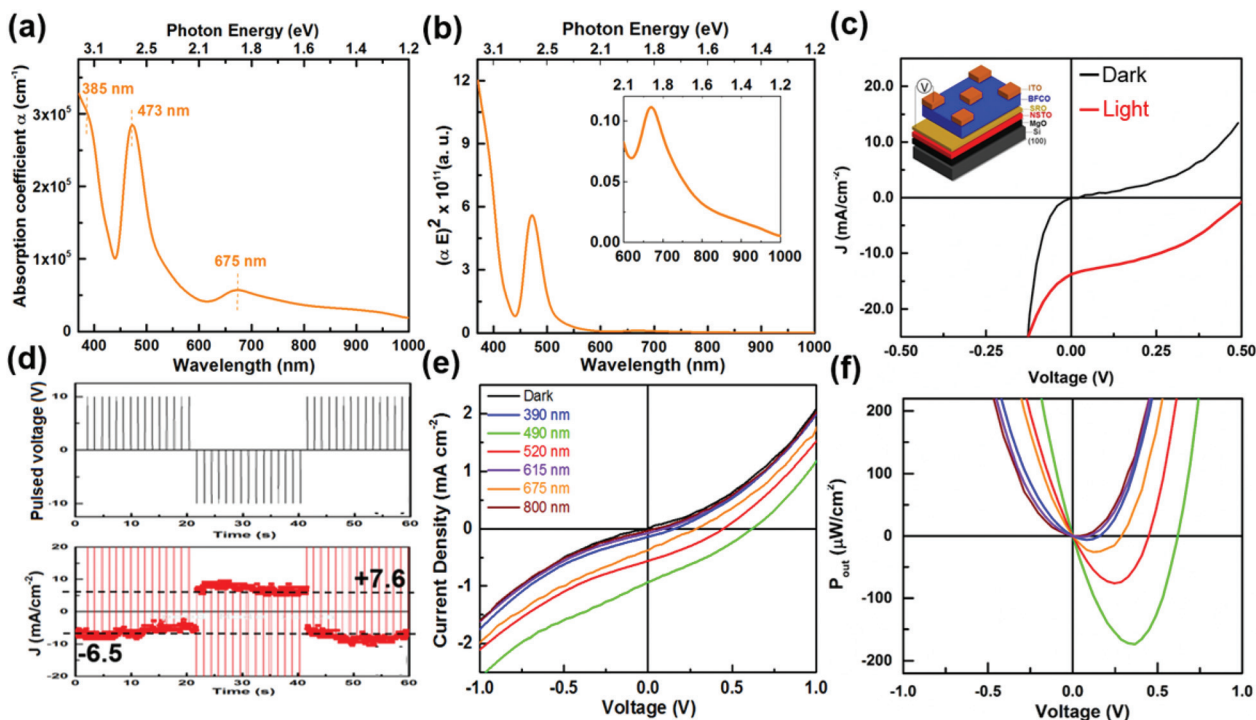
Fig. 3 (a) UV-visible absorption spectrum of the BFCO thin films. (b) Corresponding direct optical transitions of the overall BFCO thin films. The inset shows the enlarged curve at higher wavelength. (c) $J-V$ curves of 200 nm thick BFCO thin films grown on Si(100) under 1 Sun illumination. (d) PV response of the heterostructure under pulsed voltage evidencing the bulk PV effect of BFCO. The values $-6.5$ and $7.6$ mA cm$^{-2}$ are short circuit current densities obtained for BFCO films after being positively ($+10$ V) and negatively poled ($-10$ V) (e) PV measurements of the positively poled BFCO films at different wavelengths and (f) the corresponding generated power densities.

and BCO[28] thin films. Since light absorption and carrier concentrations are both band-gap dependent, the red-shift of the absorption edge of BFCO with respect to BCO and BFO and the increase of the spectral weight around 1.55 and 2.14 eV will increase the power conversion efficiencies (PCE) recently reported in such oxide materials (typically between 0.1 and 0.3%).[29–31]

We studied the PV properties of BFCO thin films integrated on a Si substrate under 1.5 AM Sunlight, corresponding to an incident power density of 100 mW cm$^{-2}$. Device characterization was carried out in an ambient environment. The current–voltage characteristics of the electric devices were recorded using a Keithley source meter. 1 Sun illumination was obtained by using an AAA class Sun simulator equipped with a 1.5 AM filter with an irradiation intensity of 100 mW cm$^2$. The wavelength dependent PV measurements were acquired using a monochromator (Oriel integrated system). To avoid electrical breakdown, 2D arrays of indium doped tin oxide (ITO) transparent electrodes were deposited to perform electrical measurements at different locations on the device. The active area of the device is around $0.25 \times 0.25$ mm$^2$. As shown in Fig. 3a, the device exhibits short circuit current density ($J_{sc}$) and open circuit photovoltage ($V_{oc}$) values of 13.8 mA cm$^{-2}$ and 0.52 V, respectively, at a fill factor (FF) of 0.38. A PCE of 2.65% was obtained from BFCO based PV devices. Besides the $V_{oc}$, the other PV parameters are close to

those reported for single component BFCO layer devices and largely exceed those obtained for BFO.[8,29] These devices generated a higher $V_{oc}$ of about 0.79 V, which contributes to obtain a PCE value of 3.3%. We believe that the reduced photovoltage is due to the low diffusion length of photogenerated charge carriers in the BFCO material where the ferroelectric domains are predominantly oriented in-plane and thus do not contribute efficiently to the photocharge separation process. A series of $\pm10$ V pulses were applied to pole the devices and the current response was then measured in the dark and under 1.5 AM illumination and at zero applied voltage (Fig. 3d). The direction of the photocurrent is strongly dependent on the poling direction; this is a signature of excited carrier separation in the bulk exhibited by ferroelectrics. The polarization direction modulates the height barrier at the interfaces which affect directly the displacement of photogenerated electron–hole pairs and thus control the direction of the photogenerated current flow.[8] The contribution from ferroelectricity is evidenced by the reversibility of the short circuit photocurrent with respect to switching the ferroelectric polarization direction (Fig. 3d). The obtained short circuit photocurrent density values after negative and positive poling are close, suggesting that the contribution of the polarization induced-internal electrical field to the photocurrent is predominant.

We also examined the dependence of the photocurrent response of the BFCO-based device on the incident optical

wavelength, using a monochromatic source tunable from 300 to 1800 nm (Fig. S2a†). The PV response starts to rise at about 800 nm (1.55 eV) with peaks at about 675 nm (1.83 eV) and 490 nm (2.53 eV), thus representing a good match with the absorption spectrum (Fig. 3a). Measurements of the $V_{oc}$ and $J_{sc}$ indicate that the photoresponse of the BFCO-based device is optimal under 490 nm wavelength illumination. The dependence of the absorption coefficient on wavelength causes different wavelengths to penetrate different distances (*cf.* Fig. S2b†) into the BFCO film before most of the light is absorbed. As illustrated in Fig. S2b,† the absorption depth, which corresponds to the inverse of the absorption coefficient for 490 nm and 615 nm was found to be around 30 nm and 240 nm, respectively. On the basis of the thickness of the 200 nm BFCO film, 615 nm wavelength light will not be absorbed, thereby dramatically reducing the photoresponse of the device, as evidenced by the *J–V* curves (Fig. 3e). High energy light (390 nm) is absorbed within a short distance from the surface, whereas red (higher than 700 nm) is absorbed less efficiently, which explains the poor PV performance of the devices under these illuminations. Nevertheless, the BFCO based devices were able to generate power densities up to 180 μW cm$^{-2}$ (Fig. 3f). Recent advances in low-power microelectronic designs have resulted in very small power requirements of only 10–100 μW.[32] The generated power values may enable the use of BFCO based devices to harvest energy for wireless applications, eliminating the need for bulkier, higher cost batteries or expensive and complex wiring.[33,34] Our results suggest that BFCO is a promising candidate for energy harvesting and powering multiple applications including *e.g.* wireless sensor networks.

In summary, epitaxial BFCO thin films were grown on silicon substrates using an MgO buffer layer. The BFCO films crystallize in a single phase and are highly *c*-oriented. 200 nm thick films mainly exhibited a tensile strained phase with IP and OP lattice parameters of 3.98 Å and 3.89 Å, respectively. As evidenced by XRD measurements, there is a fraction of cationic ordering between Fe and Cr in BFCO films. Since theoretical predictions about the crystal structure of BFCO with Fe/Cr valence states are different from 3+, we are not able to estimate exactly the percentage of Fe/Cr cationic ordering in our films. PFM measurements revealed that the tensile strained BFCO phase exhibits a polarization predominantly oriented through the IP direction. The relaxation of this tensile strain results in the appearance of an OP component for the ferroelectric polarization. The semiconducting bandgap of the ordered BFCO phase combined with its ferroelectric properties, opens the possibility of PCE above 2% in a thin film device and the use of ferroelectric materials simultaneously as solar absorber layers and carrier separators in PV devices.

Further investigations are under way to establish strategies to increase the fill factor and the photovoltage and increase the PV efficiency in such devices. More work is needed to achieve the integration of BFCO thin films in tandem geometry with a silicon cell, since the optimum tandem cell requires suitable matching of the generated currents by the top and bottom cells at closer fill factors.

## Acknowledgements

## References

1 M. Alexe and D. Hesse, *Nat. Commun.*, 2011, **2**, 256.
2 J. P. Chakrabartty, R. Nechache, C. Harnagea and F. Rosei, *Opt. Express*, 2014, **22**, A80–A89.
3 W. Ji, K. Yao and Y. Liang, *Adv. Mater.*, 2010, **22**, 1763.
4 R. Nechache, C. Harnagea, S. Licoccia, E. Traversa, A. Ruediger, A. Pignolet and F. Rosei, *Appl. Phys. Lett.*, 2011, **98**, 202902.
5 R. Nechache, C. V. Cojocaru, C. Harnagea, C. Nauenheim, M. Nicklaus, A. Ruediger, F. Rosei and A. Pignolet, *Adv. Mater.*, 2011, **23**, 1724.
6 S. Y. Yang, J. Seidel, S. J. Byrnes, P. Shafer, C.-H. Yang, M. D. Rossell, P. Yu, Y.-H. Chu, J. F. Scott, J. W. Ager, L. W. Martin and R. Ramesh, *Nat. Nanotechnol.*, 2010, **5**, 143–147.
7 M. Qin, K. Yao and Y. C. Liang, *Appl. Phys. Lett.*, 2008, **93**, 122904.
8 R. Nechache, C. Harnagea, S. Li, L. Cardenas, W. Huang, J. Chakrabartty and F. Rosei, *Nat. Photonics*, 2015, **9**, 61–67.
9 Z. M. Beiley and M. D. McGehee, *Energy Environ. Sci.*, 2012, **5**, 9173–9179.
10 R. Nechache, A. Ruediger and F. Rosei, *US Pat.*, US20120017976 A1, 2012.
11 W. Shockley and H. J. Queisser, *J. Appl. Phys.*, 1961, **32**, 510–519.
12 M. A. Green, *IEEE Trans. Electron Devices*, 1984, **5**, 671–678.
13 N. N. La, T. P. White and K. R. Catchpole, *IEEE J. Photovoltaics*, 2014, **4**, 208.
14 T. Abukawa, S. Sato and Y. Matsuoka, *Surf. Sci.*, 2010, **604**, 1614–1618.
15 J. Wang, H. Zheng, Z. Ma, S. Prasertchoung, M. Wuttig, R. Droopad, J. Yu, K. Eisenbeiser and R. Ramesh, *Appl. Phys. Lett.*, 2004, **85**, 2574–2576.

16 S. G. Yoon, in *Ferroelectrics*, ed. I. Coondoo, InTech, 2010, ISBN: 978-953-307-439-9.

17 H. N. Lee, S. Senz, A. Pignolet and D. Hesse, *Appl. Phys. Lett.*, 2001, **78**, 2922.

18 T. I. Chen, X. M. Li, S. Zhang and X. Zhang, *Appl. Phys. A*, 2005, **80**, 73.

19 R. Nechache and F. Rosei, *J. Solid State Chem.*, 2012, **189**, 13–20.

20 P. Baettig and N. A. Spaldin, *Appl. Phys. Lett.*, 2005, **86**, 012505.

21 C. Harnagea, C. V. Cojocaru, O. Gautreau, R. Nechache, F. Normandin, T. Veres and A. Pignolet, *Integr. Ferroelectr.*, 2006, **83**, 1.

22 A. Rana, K. Bogle, Q. Zhang, R. Vasudevan, N. Valanoor, V. Thakare, S. Ogale, H. Lu and A. Gruverman, *Adv. Funct. Mater.*, 2014, **24**, 3962.

23 J. Tauc, R. Grigorovici and A. Vancu, *Phys. Status Solidi B*, 1966, **15**, 627.

24 T. P. Gujar, V. R. Shinde and C. D. Lokhande, *Mater. Chem. Phys.*, 2007, **103**, 142.

25 J. Andreasson, J. Holmlund, S. G. Singer, C. S. Knee, R. Rauer, B. Schulz, M. Käll, M. Rübhausen, S. G. Eriksson, L. Börjesson and A. Lichtenstein, *Phys. Rev. B: Condens. Matter*, 2009, **80**, 075103.

26 A. Ohtomo, S. Chakraverty, H. Mashiko, T. Oshima and M. Kawasaki, *J. Mater. Res.*, 2013, **28**, 689–695.

27 C. Himcinschi, I. Vrejoiu, M. Friedrich, E. Nikulina, L. Ding, C. Cobet, N. Esser, M. Alexe, D. Rafaja and D. R. T. Zahn, *J. Appl. Phys.*, 2010, **107**, 123524.

28 C. Himcinschi, I. Vrejoiu, T. Weißbach, K. Vijayanandhini, A. Talkenberger, C. Röder, S. Bahmann, Di. R. T. Zahn, A. A. Belik, D. Rafaja and J. Kortus, *J. Appl. Phys.*, 2011, **110**, 073501.

29 F. Zheng, Y. Xin, W. Huang, J. Zhang, X. Wang, M. Shen, W. Dong, L. Fang, Y. Bai, X. Shen and J. Hao, *J. Mater. Chem. A*, 2014, **2**, 1363.

30 J. P. Chakrabartty, R. Nechache, C. Harnagea and F. Rosei, *Opti. Express*, 2014, **22**, A80–A89.

31 J. Chakrabartty, R. Nechache, S. Li, M. Nicklaus, A. Ruediger and F. Rosei, *J. Am. Ceram. Soc.*, 2014, **97**, 1837–1840.

32 H. R. Trankler and O. Kanoun, Proceedings of the 18th IEEE Instrumentation and Measurement Technology Conference, 2001, pp. 309–316.

33 S. Meninger, J. O. Mur-Miranda, R. Amirtharajah and A. P. Chandrakasan, *IEEE Trans. VLSI Syst.*, 2001, **9**, 64–76.

34 W. R. Davis, N. Zhang, K. Camera, F. Chen, B. Nikolic and R. Brodersen, Proceedings of the IEEE Custom Integrated Circuits Conference, 2001, San Diego, CA, USA.